Quantum Networks Enhanced by Distributed Quantum Memories

Xiangyi Meng,[1] Nicolò Lo Piparo,[2] Kae Nemoto,[2] and István A. Kovács[1, 3, 4, *]

[1]*Department of Physics and Astronomy, Northwestern University, Evanston, Illinois 60208, USA*
[2]*Okinawa Institute of Science and Technology Graduate University,*
1919-1 Tancha, Onna-son, Okinawa 904-0495, Japan
[3]*Northwestern Institute on Complex Systems, Northwestern University, Evanston, Illinois 60208, USA*
[4]*Department of Engineering Sciences and Applied Mathematics,*
Northwestern University, Evanston, Illinois 60208, USA
(Dated: March 26, 2024)

Building large-scale quantum communication networks has its unique challenges. Here, we demonstrate that a network-wide synergistic usage of quantum memories distributed in a quantum communication network offers a fundamental advantage. We first map the problem of quantum communication with local usage of memories into a classical continuum percolation model. Then, we show that this mapping can be improved through a cooperation of entanglement distillation and relay protocols via remote access to distributed memories. This improved mapping, which we term α-percolation, can be formulated in terms of graph-merging rules, analogous to the decimation rules of the renormalization group treatment of disordered quantum magnets. These rules can be performed in any order, yielding the same optimal result, which is characterized by the emergence of a "positive feedback" mechanism and the formation of spatially disconnected "hopping" communication components—both marking significant improvements in quantum network connectivity.

TABLE I: Glossary of the equivalent problem representations.

Variables: r_a, d_{bc}	$(r')^{1/\alpha} = r_a^{1/\alpha} + r_b^{1/\alpha}$ [Eq. (4)]	$d'_{bc} = \min\{d_{bc}, d_{ab} + d_{ac}\}$ [Eq. (6)]
Communication protocol	remote distillation	quantum relay
Graph-merging rules	contraction	reduction
α-percolation	positive feedback	hopping

Rapid advancements in quantum communication technologies [1] call for a better understanding of the potential benefits of using *quantum memory* elements, a key resource constraint [2]. Quantum memories, akin to their classical counterparts, play an essential role in enabling the parallel processing of mixed states, which are inherently probabilistic. For example, the one-shot entanglement purification protocol [3], designed to transform two less entangled pairs of qubits into a single pair with stronger entanglement, only succeeds with a success probability $p < 1$. This fundamental stochasticity poses considerable complexity in scaling up to *entanglement distillation* from n pairs in a nested way, which includes a total of $O(n)$ one-shot purification steps as building blocks [3]. Without quantum memories, all $O(n)$ purification steps must succeed simultaneously. As a result, the average waiting time to witness a successful outcome extends to $O(p^{-n})$, assuming that p is the same for all steps. On the other hand, with sufficient $O(n)$ memories, all purification steps can be executed concurrently when distilling $n/2$ pairs from n pairs each time. This way, the whole process takes only $O(\log_2 n)$ rounds, significantly reducing the time complexity to $O(p^{-\log_2 n}) = O(n^{-\log_2 p})$, a polynomial in n [3].

This example illustrates that entanglement can be feasibly enhanced within subexponential time complexity between two parties equipped with memories, leading to higher entanglement generation rates. This enhancement, however, becomes less transparent in the context of a spatial network, where memories are not concentrated but *distributed* across multiple parties (nodes), resembling modern distributed computing architectures [4]. Since access to remotely distributed memories also costs entanglement resources, a critical question arises: *can distributed quantum memories offer major enhancements in quantum communication networks?* Surprisingly, despite the rich literature on quantum networks [5], there lacks a general network model for distributed quantum memories, which should be characterized as node weights in the network. This sets the model apart from other well-developed link-weighted quantum network models, such as photonic communication [6], channel capacity bounds [7], or entanglement percolation theories [8].

In this Letter, we bridge this gap by first mapping the problem of quantum communication with distributed memories to a classical *continuum percolation* model [9], where the number of memories at each node directly maps to the node's "range." Quantum communication is then only possible within connected components, formed by nodes within each other's range. We further show that a node can, indeed, achieve a greater range by

* istvan.kovacs@northwestern.edu

utilizing distributed memories from other nodes in the same component, a benefit that outweighs the cost of accessing them. This results in a modified percolation model, which we term α-*percolation*, that has a single parameter, α, representing the efficiency of the communication protocols involved. We show that α-percolation can be formulated through two graph-merging rules (Table I). With the right prescription, any order of applying the rules leads to the same optimal, final configuration that marks a substantial enhancement in network connectivity, manifesting through both model and real fiber network topologies.

Continuum percolation mapping.—We start by considering a collection of N nodes *without* memories, each spatially embedded such that a distance d_{ij} is defined between every two nodes i and j, measuring for instance the length of optical fibers connecting the nodes. Each node uses flying qubits (e.g., photons) to establish bipartite entanglement with other nodes. These flying qubits are considered to be cheap and abundant in quantity (assuming they are protected by a heralding mechanism [10]), but compromised in quality when they transmit through noisy, distance-dependent quantum channels. We model these channels by the depolarizing channel, a universal, worst-case noise model [11]. The outcome of the depolarizing channel is a bipartite mixed isotropic state (Werner state) [12] that links nodes i and j, described by the density matrix,

$$\rho(d_{ij}) = p(d_{ij}) \left| \Psi^- \right\rangle \left\langle \Psi^- \right| + (1 - p(d_{ij})) \, \mathbf{I}/4. \quad (1)$$

Here, $\mathbf{I}$ is the identity matrix, representing the state of maximum noise, and $\left| \Psi^- \right\rangle \left\langle \Psi^- \right|$ is a maximally entangled state between two qubits, specifically one of the four Bell states. The distance dependence of the coefficient $p(d_{ij})$ is modeled by an exponential decay, $p(d_{ij}) = e^{-d_{ij}/d_0}$, where d_0 signifies the characteristic decoherence distance, dictated by current technological constraints and limited to hundreds of kilometers [13].

For practical quantum communication, the fidelity between the noisy state $\rho(d_{ij})$ and the ideal state $\left| \Psi^- \right\rangle \left\langle \Psi^- \right|$, given by $F(d_{ij}) = \left(3p(d_{ij}) + 1\right)/4$, must be sufficiently close to unity. We thus seek to reach a fidelity threshold $F_{\mathrm{th}} \equiv 1 - \epsilon$ where ϵ represents a small error typically required to be smaller than 1% [14]. This allows us to introduce a uniform, constant range for every node, $r_0 = -d_0 \ln\left(1 - 4\epsilon/3\right)$, such that two nodes can directly establish usable entanglement only if $d_{ij} < r_0$. For $\epsilon \ll 1$ this formula simplifies to $r_0 \simeq 4\epsilon d_0/3$. When $d_{ij} > r_0$, the level of entanglement is insufficient to meet the fidelity threshold ($F(d_{ij}) < F_{\mathrm{th}}$). This consideration thus maps to continuum percolation: around each node i, a disk with a fixed, uniform radius r_0 is placed; only when two disks can reach each other's center [15], they forge a link, which results in a connected component.

Enhancement from quantum memories.—Now we consider the case where each node is equipped with m long-life, repeatedly usable quantum memories (e.g., NMR,
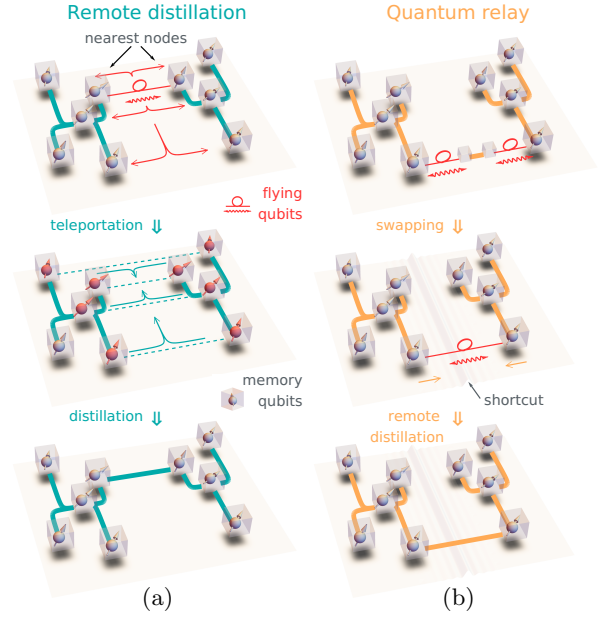

FIG. 1: Quantum communication enhanced by distributed memories. (a) Quantum memories distributed across two connected components (the "X"- and "Y"-shaped) effectively act as "cloud storage" for remotely storing flying qubits generated between the nearest nodes of the two components. This allows distillation between the two components, potentially forging a new high-entanglement link ($F > F_{\mathrm{th}}$). (b) A connected component can also act as a relay to swap flying qubits between its neighbors. This "shortcut" further promotes remote distillation to forge new links.

defect, or superconducting qubits). Already at first glance, incorporating quantum memories brings a notable improvement: between every two nodes, a pair of stronger entanglement can now be distilled within polynomial time $O(m^{-\log_2 p})$. Specifically, when merging two pairs with a fidelity of F, utilizing the BBPSSW distillation protocol [16], a new pair is created with a fidelity of F' that follows $1 - F' \simeq (2/3)\left(1 - F\right)$ in the limit $F \to 1$, which is asymptotically the same for the DEJMPS protocol [17]. Consequently, with a maximum of m pairs that can be stored, the final fidelity F' scales as $1 - F' = \epsilon \simeq (2/3)^{\log_2 m}\left(1 - F\right)$. Therefore, each initial pair before distillation only needs to achieve a fidelity of $1 - (3/2)^{\log_2 m} \epsilon$. This increases each node's range to

$$r_0 = -d_0 \ln \left[1 - \frac{4}{3}\epsilon m^{\log_2(3/2)} \right] \simeq \frac{4}{3}\epsilon m^{\alpha^*} d_0, \quad (2)$$

where $\alpha^* \equiv \log_2 (3/2) \approx 0.585$. As we show next, enhancements are not confined to the local scope of individual nodes, but also prevail at the *component* level. As nodes form larger components, there are (at least) two additional improvements:

(1) Remote distillation. Let us consider two components a and b, with respective sizes (numbers of nodes)

s_a and s_b. The total number of distributed quantum memories within these components are proportional to ms_a and ms_b, effectively functioning as "cloud storage" for storing flying qubits established through the nearest nodes between a and b (SI, Sec. I). The links within each component have high fidelity and thus can teleport the flying qubits from the nearest nodes to other nodes to store them [Fig. 1(a)]. These stored qubits are further distilled with the help of remote gate teleportation [18], resulting in a single entangled pair with an even higher fidelity that scales as $1 - F' = \epsilon \simeq (2/3)^{\log_2 n} (1 - F)$. Here, the total number of stored pairs n, which are to be distilled, depends on the *smaller* number of available memories in the two components, given by $n = \min\{ms_a, ms_b\}$. Essentially, this remote distillation allows us to rewrite the connection criterion, $d_{ij} < r_0$, to

$$\min_{i \in a, j \in b} d_{ij} < \min\{r(s_a), r(s_b)\}, \qquad (3)$$

where $r(s)$ denotes the new range of a node in a component of size s, calculated as $r(s) \simeq 4\epsilon m^\alpha s^\alpha d_0/3$, meaning that each node within a component of size $s > 1$ has a range exceeding r_0 in Eq. (2). Here, instead of a fixed α^*, we assume a generic value $\alpha > 0$.

The newly forged link between components a and b, in turn, allows the sharing of memories between a and b. As a result, the two components are now merged into a larger component of size $s_a + s_b$, implying that every node within this enlarged component gains a uniform, increased range $r' = r(s_a + s_b)$, given by

$$(r')^{1/\alpha} = r_a^{1/\alpha} + r_b^{1/\alpha}, \qquad (4)$$

where $r_a \equiv r(s_a)$ and $r_b \equiv r(s_b)$ [Fig. 2(a)]. During this process, at most $\sim n^2$ existing high-entanglement links are costed. This gives rise to a time complexity $f(n) = O(n^{\log_2 n})$ (SI, Sec. III), greater than $O(n^{-\log_2 p})$ but still *subexponential* in n, thus underscoring the enhancement by quantum memories at the component level.

Equivalently, we can view each component as a single effective node a of range r_a and define the distance between two effective nodes as $d_{ab} = \min_{i \in a, j \in b} d_{ij}$. This effective-node picture simplifies the criterion Eq. (3) to

$$d_{ab} < \min\{r_a, r_b\}. \qquad (5)$$

(2) Quantum relays. A component can also function as a quantum relay [19] and swap flying qubits between its nodes [Fig. 1(b)] by entanglement swapping [20]. Thus, given a component a, each pair of its neighboring components (denoted by b, c) can form an entangled pair, as if b and c formed a "shortcut" through a [Fig. 2(b)]. This relay function does not require, or benefit from, quantum memories (SI, Sec. II), but it may enhance further remote distillation by potentially decreasing the distance between every pair of a's neighbors to

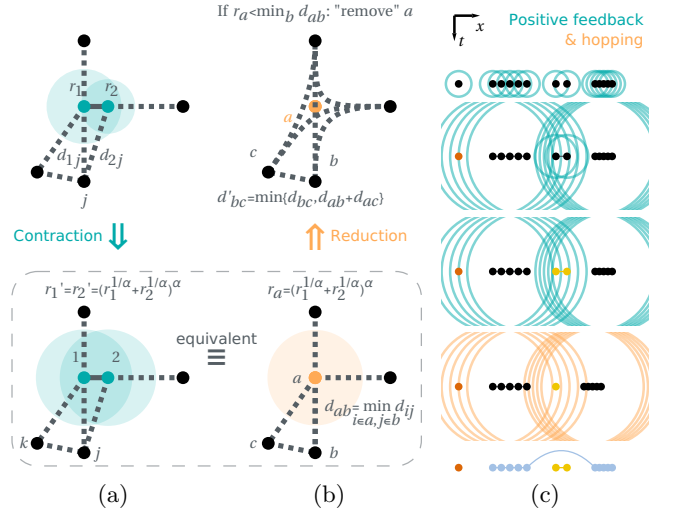$$d'_{bc} = \min\{d_{bc}, d_{ab} + d_{ac}\}. \qquad (6)$$

FIG. 2: α-percolation with graph rules. (a) The contraction rule [Eq. (4)] redefines a uniform range for every node within the same component, which is equivalent to contracting $1, 2, \cdots$ into a single "effective node" a of range r_a. (b) The reduction rule [Eq. (6)] "removes" an effective node a but creates a shortcut between each pair of its neighbors $(b, c, \cdots)$. This only happens when a is isolated ($r_a < \min_b d_{ab}$). (c) During the α-percolation process (from top to bottom), nodes within mutual reach are joined as a larger component, which in turn increases each node's new range (denoted by the circles' radii), representing a "positive feedback" mechanism. When a component is isolated and removed (highlighted in distinct colors, e.g., the yellow nodes), it can still provide shortcuts that may facilitate "hopping" links (e.g., the blue link) between other components.

Equation (6) is derived from the fact that given two entangled pairs, one between a, b and the other between a, c, entanglement swapping [21] at the effective node a (more precisely, at all nodes $i \in a$ which are along the path connecting b and c) gives $p'_{bc} = p(d_{ab})p(d_{ac})$ by Eq. (1), thus yielding the term $d_{ab} + d_{ac}$ in Eq. (6). Moreover, given that flying qubits are abundant, if there is already a channel between b and c (characterized by d_{bc}), only the shortest link connecting the two components contributes to further distillation processes. This warrants the minimum rule in Eq. (6) (SI, Sec. II).

While Eq. (6) can be repeatedly applied, optimal connectivity is achieved by invoking Eq. (6) once—and for all—on a component a immediately after its range is not large enough to reach any other component, i.e., $r_a < \min_b d_{ab}$. This component will never be able to merge with other components again, becoming isolated and "removed," no longer participating in the percolation process (SI, Sec. IV). Eventually, all nodes become isolated, reaching the final state of percolation.

Taken together, we arrive at α-percolation, for which the new connection criterion is given by Eq. (5).

Graph rules.—α-percolation integrates two rules: the
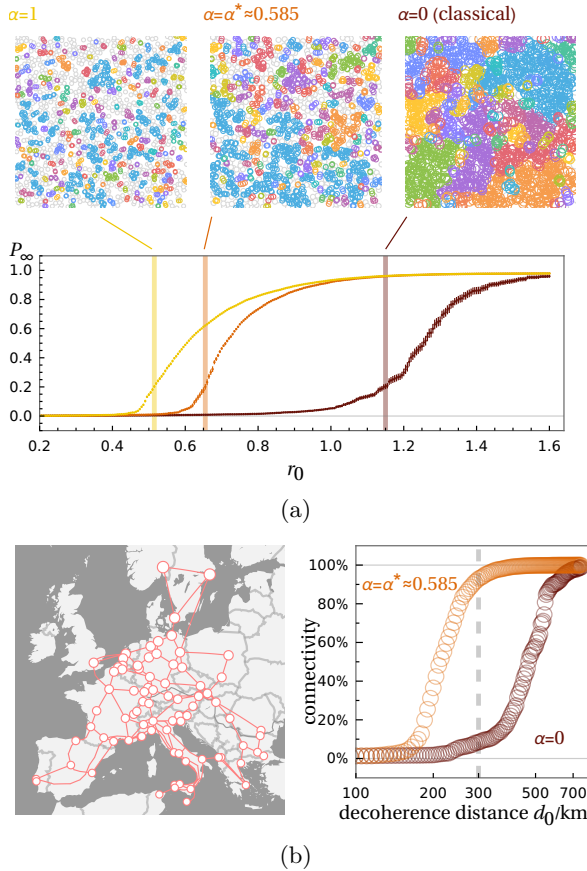
(a)

(b)

FIG. 3: α-percolation on two-dimensional networks. (a) Square lattice. As the coefficient α increases, not only does the threshold $r_0^{\rm th}$ decrease (brown to yellow), but also the giant component (of relative size P_∞) at criticality exhibits a more nonlocal and sparser distribution across space. Here, each node is illustrated using its initial range r_0, rather than the actual range $r(s)$. Components with size $s > 1$ are highlighted in distinct colors. (b) Pan-European fiber network, consisting of 692 nodes (including both stations and repeaters) and 733 links (fiber optic cables). The fidelity bound is set at $1 - \epsilon = 99\%$. Each node is assigned $m \approx 102$ quantum memories such that $m^{\alpha^*} \approx m^{0.585} = 15$.

while operating on distinct mechanisms, positive feedback phenomena have been explored in explosive percolation [23] and interdependent cascading failures [24], while the hopping feature has been investigated in tunneling continuum percolation [25] and extended-range percolation [26]. Yet, to our knowledge, the combined exploration of these two features has not been explored.

The positive feedback and hopping features become especially pronounced when r_0 approaches the percolation threshold, $r_0^{\rm th}$. At the threshold, the emerging giant component (highlighted in blue) tends to be more nonlocal and sparser as α increases [Fig. 3(a)]. Intriguingly, only one parameter α enters the model and affects both $r_0^{\rm th}$ and the distribution pattern of the giant component. In contrast, the number of memories per node, m, merely rescales r_0 [Eq. (2)] without altering the underlying percolation mechanism. Classical continuum percolation can be recovered as the $\alpha \to 0$ limit.

Our theoretical framework is predicated on taking $\epsilon \to 0$ with ϵd_0 fixed before taking the thermodynamic limit $N \to \infty$. When considering finite ϵ and d_0, an additional length scale, $\beta = d_0 \ln 3$, becomes relevant, which effectively caps a node's enhanced range $r(s)$ such that it cannot exceed β. The physical reason behind this is that in Eq. (1), any distance d_{ij} longer than $d_0 \ln 3$ suffers from entanglement sudden death [27], leading to absolute zero entanglement in the flying qubits.

Real-world fiber network.—We demonstrate potential practical applications by examining Sparkle's pan-European fiber network [28]. To bring the length scale under the threshold of β, we inserted full-fledged quantum repeaters [29] along longer cables as additional nodes. This modified the network topology by dividing cables into shorter, random segments that follow a Poisson distribution in length, averaged around 50 km. As Fig. 3(b) shows, with practically reasonable levels of fidelity and quantum memory capacity, the enhanced model ($\alpha = \alpha^*$) forecasts over 90% connectivity under the current laboratory limit of decoherence distance, $d_0 \sim 300$ km [30]. This stands in stark contrast to using only local memories ($\alpha = 0$), which would require a d_0 exceeding 600 km. This comparison underscores the critical role of integrating distributed quantum memories in practical quantum communication networks (SI, Sec. VI).

Discussion.—Our work established the profound role of quantum memories on the connectivity of quantum communication networks through mapping to a percolation process with associated graph rules. A combination of the contraction and reduction rules also appears in variants of the strong-disorder renormalization group (SDRG)—an efficient spatial renormalization group technique to generate the ground state and low-energy excitations of heterogeneous quantum systems, especially in the vicinity of quantum phase transitions [31, 32]. As recently shown, positive feedback and hopping features also emerge in SDRG, even though the precise details depend on the studied systems, such as Ising [33], Heisenberg [34], and Josephson junctions [35]. In these

contraction [Eq. (4)] and *reduction* [Eq. (6)] rules, named after their resemblance to graph-merging operations [22]. Examining these rules suggests that they can be conducted on different nodes in an arbitrary order, leading to the same final state of optimal connectivity (SI, Sec. V). This graph representation immediately reveals two key features: firstly, a "positive feedback," such that nodes within larger components achieve a greater range [shown as bigger circles in Fig. 2(c)], therefore more likely to form even larger components; secondly, "hopping" over isolated components, such that two components of no adjacency can still be connected [e.g., the blue bridge link in Fig. 2(c)]. Note that analogous features have been separately studied in the percolation literature:

models, strong heterogeneity often gives rise to the emergence of exotic disordered universality classes and Griffiths phases. It is an exciting future direction to explore whether the critical phenomena in our model are similarly influenced by heterogeneity in each node's initial range r_0.

Moreover, given a component of size s, we do not have to use all ms distributed memories but only a proportion of them, ms^η, with $\eta \leq 1$ acting as a tunable parameter. This adjustment effectively reduces the number of pairs to be distilled from n to n^η, thus altering α to $\eta\alpha$. As a trade-off, the time complexity is also reduced to $f(n) = O(n^{\eta^2 \log_2 n})$. This tunability opens up the possibility of adjusting α between 0 and α^*, striving for an optimal balance between efficiency and time complexity (rate). On the flip side, specific channels often have room for more efficient distillation protocols (e.g., R-state-based protocols [36]), which could lead to a higher gain of fidelity and thus $\alpha > \alpha^*$. However, some specific protocols might also offer greater success probabilities p, which could diminish the apparent benefits of probabilistic parallelization using quantum memories. This interplay between fidelity and success probability in distillation presents an area for further investigation.

[1] N. Gisin and R. Thew, Quantum communication, Nat. Photonics **1**, 165 (2007); Z.-S. Yuan, X.-H. Bao, C.-Y. Lu, J. Zhang, C.-Z. Peng, and J.-W. Pan, Entangled photons and quantum communication, Phys. Rep. **497**, 1 (2010); S. Wehner, D. Elkouss, and R. Hanson, Quantum internet: A vision for the road ahead, Science **362**, eaam9288 (2018).

[2] M. Razavi, M. Piani, and N. Lütkenhaus, Quantum repeaters with imperfect memories: Cost and scalability, Phys. Rev. A **80**, 032301 (2009); M. Afzelius, N. Gisin, and H. de Riedmatten, Quantum memory for photons, Phys. Today **68**, 42 (2015); Y. Jing and M. Razavi, Quantum Repeaters with Encoding on Nitrogen-Vacancy-Center Platforms, Phys. Rev. Appl. **18**, 024041 (2022); O. Milul, B. Guttel, U. Goldblatt, S. Hazanov, L. M. Joshi, D. Chausovsky, N. Kahn, E. Çiftyürek, F. Lafont, and S. Rosenblum, Superconducting Cavity Qubit with Tens of Milliseconds Single-Photon Coherence Time, PRX Quantum **4**, 030336 (2023); S. Gera, C. Wallace, M. Flament, A. Scriminich, M. Namazi, Y. Kim, S. Sagona-Stophel, G. Vallone, P. Villoresi, and E. Figueroa, Hong-Ou-Mandel interference of single-photon-level pulses stored in independent room-temperature quantum memories, npj Quantum Inf. **10**, 1 (2024).

[3] P. Horodecki and R. Horodecki, Distillation and bound entanglement, Quantum Inf. Comput. **1**, 45 (2001); W. Dür and H. J. Briegel, Entanglement purification and quantum error correction, Rep. Prog. Phys. **70**, 1381 (2007); D. Abdelkhalek, M. Syllwasschy, N. J. Cerf, J. Fiurášek, and R. Schnabel, Efficient entanglement distillation without quantum memory, Nat. Commun. **7**, 11720 (2016).

[4] L. F. Bittencourt, A. Goldman, E. R. M. Madeira, N. L. S. da Fonseca, and R. Sakellariou, Scheduling in distributed systems: A cloud computing perspective, Comput. Sci. Rev. **30**, 31 (2018).

[5] S.-H. Wei, B. Jing, X.-Y. Zhang, J.-Y. Liao, C.-Z. Yuan, B.-Y. Fan, C. Lyu, D.-L. Zhou, Y. Wang, G.-W. Deng, H.-Z. Song, D. Oblak, G.-C. Guo, and Q. Zhou, Towards Real-World Quantum Networks: A Review, Laser Photonics Rev. **16**, 2100219 (2022); X. Meng, X. Hu, Y. Tian, G. Dong, R. Lambiotte, J. Gao, and S. Havlin, Percolation Theories for Quantum Networks, Entropy **25**, 1564 (2023); J. Nokkala, J. Piilo, and G. Bianconi, Complex Quantum Networks: A Topical Review (2023), arxiv:2311.16265.

[6] S. Brito, A. Canabarro, R. Chaves, and D. Cavalcanti, Statistical Properties of the Quantum Internet, Phys. Rev. Lett. **124**, 210501 (2020); S. Brito, A. Canabarro, D. Cavalcanti, and R. Chaves, Satellite-Based Photonic Quantum Networks Are Small-World, PRX Quantum **2**, 010304 (2021).

[7] S. Pirandola, S. L. Braunstein, R. Laurenza, C. Ottaviani, T. P. W. Cope, G. Spedalieri, and L. Banchi, Theory of channel simulation and bounds for private communication, Quantum Sci. Technol. **3**, 035009 (2018); S. Pirandola, End-to-end capacities of a quantum communication network, Commun. Phys. **2**, 1 (2019).

[8] X. Meng, J. Gao, and S. Havlin, Concurrence Percolation in Quantum Networks, Phys. Rev. Lett. **126**, 170501 (2021); J. Liang, X. Chen, and T. Wang, Percolation Distribution in Small-World Quantum Networks, Appl. Sci. **12**, 701 (2022); O. Malik, X. Meng, S. Havlin, G. Korniss, B. K. Szymanski, and J. Gao, Concurrence percolation threshold of large-scale quantum networks, Commun. Phys. **5**, 1 (2022); X. Meng, Y. Cui, J. Gao, S. Havlin, and A. E. Ruckenstein, Deterministic entanglement distribution on series-parallel quantum networks, Phys. Rev. Research **5**, 013225 (2023).

[9] R. Meester and R. Roy, *Continuum Percolation*, 1st ed., Cambridge Tracts in Mathematics (Cambridge University Press, Cambridge, 1996).

[10] S. Muralidharan, L. Li, J. Kim, N. Lütkenhaus, M. D. Lukin, and L. Jiang, Optimal architectures for long distance quantum communication, Sci. Rep. **6**, 20463 (2016); P. C. Humphreys, N. Kalb, J. P. J. Morits, R. N. Schouten, R. F. L. Vermeulen, D. J. Twitchen, M. Markham, and R. Hanson, Deterministic delivery of remote entanglement on a quantum network, Nature **558**, 268 (2018).

[11] X. S. Yao, Devices for depolarizing polarized light (2002); C. King, The capacity of the quantum depolarizing channel, IEEE Trans. Inf. Theor. **49**, 221 (2003).

[12] R. F. Werner, Quantum states with Einstein-Podolsky-Rosen correlations admitting a hidden-variable model, Phys. Rev. A **40**, 4277 (1989).

[13] J. F. Dynes, H. Takesue, Z. L. Yuan, A. W. Sharpe,

K. Harada, T. Honjo, H. Kamada, O. Tadanaga, Y. Nishida, M. Asobe, and A. J. Shields, Efficient entanglement distribution over 200 kilometers, Opt. Express **17**, 11440 (2009); M. K. Gupta, *Minimizing Decoherence in Optical Fiber for Long Distance Quantum CommunicationQuantum Communication*, Ph.D. thesis, Louisiana State University (2016).

[14] S. J. Evered, D. Bluvstein, M. Kalinowski, S. Ebadi, T. Manovitz, H. Zhou, S. H. Li, A. A. Geim, T. T. Wang, N. Maskara, H. Levine, G. Semeghini, M. Greiner, V. Vuletić, and M. D. Lukin, High-fidelity parallel entangling gates on a neutral-atom quantum computer, Nature **622**, 268 (2023).

[15] Here, our "center-reaching" convention ($d < r_0$) differs from the traditional "periphery-reaching" convention ($d < 2r_0$), which can be achieved by replacing our r_0 by $2r_0$. However, only the center-reaching convention upholds the geometric interpretation of Eq. (5) once moving to α-percolation.

[16] C. H. Bennett, G. Brassard, S. Popescu, B. Schumacher, J. A. Smolin, and W. K. Wootters, Purification of Noisy Entanglement and Faithful Teleportation via Noisy Channels, Phys. Rev. Lett. **76**, 722 (1996).

[17] D. Deutsch, A. Ekert, R. Jozsa, C. Macchiavello, S. Popescu, and A. Sanpera, Quantum Privacy Amplification and the Security of Quantum Cryptography over Noisy Channels, Phys. Rev. Lett. **77**, 2818 (1996).

[18] S. F. Huelga, J. A. Vaccaro, A. Chefles, and M. B. Plenio, Quantum remote control: Teleportation of unitary operations, Phys. Rev. A **63**, 042303 (2001).

[19] B. C. Jacobs, T. B. Pittman, and J. D. Franson, Quantum relays and noise suppression using linear optics, Phys. Rev. A **66**, 052307 (2002); H. de Riedmatten, I. Marcikic, W. Tittel, H. Zbinden, D. Collins, and N. Gisin, Long Distance Quantum Teleportation in a Quantum Relay Configuration, Phys. Rev. Lett. **92**, 047904 (2004).

[20] M. Żukowski, A. Zeilinger, M. A. Horne, and A. K. Ekert, "Event-Ready-Detectors" Bell Experiment via Entanglement Swapping, Phys. Rev. Lett. **71**, 4287 (1993).

[21] A. Sen(De), U. Sen, Č. Brukner, V. Bužek, and M. Żukowski, Entanglement swapping of noisy states: A kind of superadditivity in nonclassicality, Phys. Rev. A **72**, 042310 (2005).

[22] B. Bollobás, *Random Graphs*, 1st ed., Cambridge Studies in Advanced Mathematics, Vol. 73 (Academic Press, London, UK, 1985); J. L. Gross and J. Yellen, *Graph Theory and Its Applications*, 2nd ed. (CRC Press, Boca Raton, FL, USA, 2005).

[23] R. M. D'Souza and J. Nagler, Anomalous critical and supercritical phenomena in explosive percolation, Nat. Phys. **11**, 531 (2015); R. M. D'Souza, J. Gómez-Gardeñes, J. Nagler, and A. Arenas, Explosive phenomena in complex networks, Adv. Phys. **68**, 123 (2019).

[24] S. V. Buldyrev, R. Parshani, G. Paul, H. E. Stanley, and S. Havlin, Catastrophic cascade of failures in interdependent networks, Nature **464**, 1025 (2010); J. Gao, S. V. Buldyrev, H. E. Stanley, and S. Havlin, Networks Formed from Interdependent Networks, Nat. Phys. **8**, 40 (2012).

[25] S. Fostner, R. Brown, J. Carr, and S. A. Brown, Continuum percolation with tunneling, Phys. Rev. B **89**, 075402 (2014).

[26] L. Cirigliano, C. Castellano, and G. Timár, Extended-range percolation in complex networks, Phys. Rev. E **108**, 044304 (2023).

[27] T. Yu and J. H. Eberly, Finite-Time Disentanglement via Spontaneous Emission, Phys. Rev. Lett. **93**, 140404 (2004); Sudden death of entanglement: Classical noise effects, Opt. Commun. **264**, 393 (2006); Q.-J. Tong, J.-H. An, H.-G. Luo, and C. H. Oh, Mechanism of Entanglement Preservation, Phys. Rev. A **81**, 052330 (2010).

[28] Sparkle, The Global Backbone Experience [http://www.globalbackbone.tisparkle.com].

[29] K. Azuma, S. E. Economou, D. Elkouss, P. Hilaire, L. Jiang, H.-K. Lo, and I. Tzitrin, Quantum repeaters: From quantum networks to the quantum internet, Rev. Mod. Phys. **95**, 045006 (2023).

[30] T. Inagaki, N. Matsuda, O. Tadanaga, M. Asobe, and H. Takesue, Entanglement distribution over 300 km of fiber, Opt. Express **21**, 23241 (2013).

[31] S. Sachdev, *Quantum Phase Transitions*, reprint ed. (Cambridge University Press, Cambridge, 2001).

[32] F. Iglói and C. Monthus, Strong disorder RG approach of random systems, Phys. Rep. **412**, 277 (2005); Strong disorder RG approach – a short review of recent developments, Eur. Phys. J. B **91**, 290 (2018).

[33] B. M. McCoy and T. T. Wu, Theory of a Two-Dimensional Ising Model with Random Impurities. I. Thermodynamics, Phys. Rev. **176**, 631 (1968); D. S. Fisher, Random transverse field Ising spin chains, Phys. Rev. Lett. **69**, 534 (1992); I. A. Kovács and F. Iglói, Renormalization group study of the two-dimensional random transverse-field Ising model, Phys. Rev. B **82**, 054437 (2010).

[34] S.-K. Ma, C. Dasgupta, and C.-K. Hu, Random Antiferromagnetic Chain, Phys. Rev. Lett. **43**, 1434 (1979).

[35] E. Altman, Y. Kafri, A. Polkovnikov, and G. Refael, Phase Transition in a System of One-Dimensional Bosons with Strong Disorder, Phys. Rev. Lett. **93**, 150402 (2004); Superfluid-insulator transition of disordered bosons in one dimension, Phys. Rev. B **81**, 174528 (2010).

[36] F. Rozpedek, T. Schiet, L. P. Thinh, D. Elkouss, A. C. Doherty, and S. Wehner, Optimizing practical entanglement distillation, Phys. Rev. A **97**, 062333 (2018).

[37] I. A. Kovács, *Infinitely Disordered Critical Behavior in Higher Dimensional Quantum Systems*, Ph.D. thesis, Eötvös Loránd University (2012).

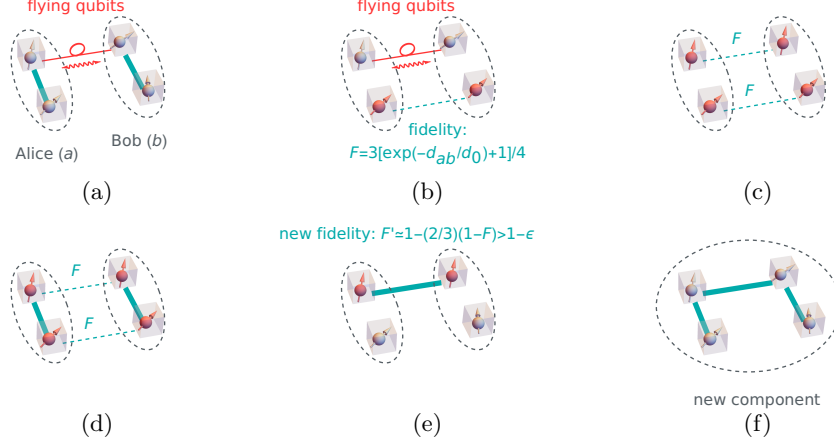**CONTENTS**

I.   REMOTE DISTILLATION

FIG. S1: Remote distillation protocol. (a) There are abundant flying qubits between the two nearest nodes of two components, Alice (a) and Bob (b). However, these flying qubits cannot be efficiently distilled without using memories. (b) At the expense of existing high-entanglement links, the flying qubits are teleported to neighboring nodes and stored in the distributed memories. (c) All flying qubits are stored. Several entangled pairs are formed in parallel between the two components. (d) The expended high-entanglement links are regenerated. (e) A new entangled pair of higher fidelity is distilled using remote gate teleportation (CNOT gates)—again, at the expense of existing high-entanglement links. The new pair can be treated as a high-entanglement link if the new fidelity is larger than the threshold, $F' > 1 - \epsilon$. (f) Existing high-entanglement links are regenerated. Now the two components merge into a larger component.

In traditional entanglement distillation protocols [3], there are n bipartite qubit pairs. Each pair is stored in memories, distributed across two parties (nodes), Alice (a) and Bob (b). The goal is to distill from these n pairs a single pair exhibiting higher entanglement. This endeavor assumes the capability of Alice and Bob to apply CNOT operations across their respective qubits [3]. However, when Alice or Bob operates as a connected component of spatially distributed real nodes, Alice (Bob) is unable to directly perform a CNOT gate on qubits that are housed in different nodes within her (his) components, due to the principle that operations across separate nodes must adhere to the restrictions of local operations and classical communication (LOCC). Consequently, the only way for Alice (Bob) to manipulate the qubits distributed across her (his) component and to perform a CNOT gate operation is through the technique of remote gate teleportation [18]. The remote gate teleportation uses the connections—existing high-entanglement links—between different nodes within the component to teleport the CNOT gate operation from one node to another. This underpins the groundwork for the implementation of our remote distillation protocol.

The process is introduced as follows (Fig. S1):

Firstly, consider two connected components, a and b, each consisting of s_a and s_b nodes that are connected by existing links. Each link represents an existing, almost-perfectly entangled pair of qubits between two nodes in the component. Our initial task involves identifying the two nearest individual nodes between the two components a and b. The reason is that the channel between the two nearest nodes gives the highest fidelity of entanglement (for now) that can be established between a and b.

The next step is to distill entanglement from this identified channel. We assume that there are abundant flying qubits in the channel. This guarantees that there are always enough entangled flying qubits to be stored into all available memories. The remote distillation protocol aims to employ not just the quantum memories housed in these two nearest nodes (assuming each node contains m quantum memories), but also those within the entire component connected to these two nodes, effectively leveraging ms_a and ms_b quantum memories in total. To accomplish this, we first employ the existing high-entanglement links to teleport qubits from the two nearest nodes to other nodes within their respective components. The maximum number of entangled pairs can be stored in memories between the two components in parallel is determined by $n = \min\{ms_a, ms_b\}$. This teleportation step costs the high-entanglement links within the components, and thus one needs to wait for the regeneration of the links. Consequently, this regeneration introduces additional time complexity to the remote distillation protocol compared to traditional distillation protocols using local memories. The implications of this time complexity will be further discussed through a one-dimensional example in Section III.

Once the parallel storage of entangled pairs between components a and b is achieved, the subsequent phase involves teleporting and executing CNOT operations across all nodes in the two components that have entangled pairs stored. This action, again, costs the high-entanglement links within the network, thereby adding an additional layer of time complexity to the process.

Utilizing these teleported CNOT operations enables the creation of a pair of qubits with higher entanglement between the two nearest nodes. Taking the BBPSSW distillation protocol for example [16], each of the n entangled pairs stored within quantum memories is represented as an isotropic state described by:

$$\rho \;=\; p\left|\Psi^-\right\rangle\left\langle\Psi^-\right| + (1-p)\,\mathbf{I}/4, \tag{S1}$$

where

$$p = e^{-d_{ab}/d_0} \tag{S2}$$

is a function of the minimum distance d_{ab} between components a and b—specifically, the distance between their two nearest nodes—relative to a characteristic length d_0. The fidelity of such a pair is calculated as $F = \langle\Psi^-|\,\rho\,|\Psi^-\rangle = (3p+1)/4$ [12]. Using the BBPSSW distillation protocol [16], two pairs of fidelity F are merged into a new pair with an enhanced fidelity:

$$F' = \frac{F^2 + \frac{1}{9}\left(1-F\right)^2}{F^2 + \frac{2}{3}F\left(1-F\right) + \frac{5}{9}\left(1-F\right)^2}. \tag{S3}$$

In the limit $F \to 1$, one has $1 - F' \simeq (2/3)\left(1-F\right)$. Implementing the BBPSSW protocol in a recursive manner—initially with n pairs, then with $n/2$ after the first iteration, and so on—allows for a progressive enhancement of fidelity. The final fidelity will be given by:

$$1 - F_{\text{final}} \simeq (2/3)^{\log_2 n}\left(1-F\right). \tag{S4}$$

If the final pair's entanglement exceeds the fidelity threshold we set, $F_{\text{final}} \geq 1 - \epsilon$, we treat this pair as a new high-entanglement link, which can be further used for teleportation purposes.

With the establishment of a new high-entanglement link, the previously separate components a and b now effectively merge into a larger component. This process allows for the recursive application of the remote distillation protocol, thereby fostering a positive feedback (as discussed in the main text). Within the framework of continuum percolation theory, as we approach the limit of $\epsilon \to 0$, the positive feedback amounts to the increase of the reaching "range" of this larger component, which can be succinctly expressed as:

$$(r')^{1/\alpha} = r_a^{1/\alpha} + r_b^{1/\alpha}, \tag{S5}$$

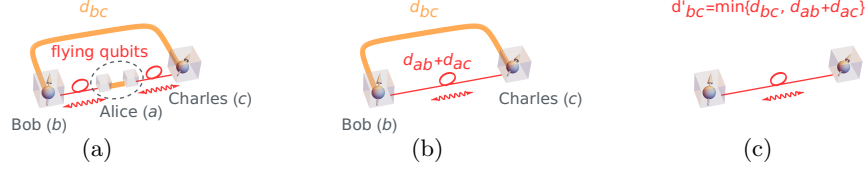which is the *contraction rule* highlighted in the main text.

II. QUANTUM RELAY

FIG. S2: Quantum relay protocol. (a) There are abundant flying qubits between Alice (a) and Bob (b), as well as Alice (a) and Charlies (c). (b) Entanglement swapping protocol on a creates a direct channel between b and c, with effective distance $d_{ab} + d_{ac}$. (c) The shortest channel produces the highest-fidelity flying qubits. Thus, only the shortest channel is kept.

A quantum relay protocol [19] exclusively relies on Bell-basis entanglement swapping [20, 21] applied to mixed states. The process is introduced as follows (Fig. S2):

Consider three nodes, Alice (a), Bob (b), and Charles (c) in the network. Alice and Bob share a pair of flying qubits in the form of the isotropic state [Eq. (S1)], with fidelity F_{ab}, or $p_{ab} = (4F_{ab} - 1)/3$. Similarly, Alice and Charles share a pair of flying qubits in the isotropic state, with fidelity F_{ac}, or $p_{ac} = (4F_{ac} - 1)/3$. A successful Bell-basis entanglement swapping requires a Bell-state measurement on the two flying qubits that Alice holds, followed by classical communication to Bob and Charles, which then leads to local transformations on Bob's and Charles's own qubits [20]. Given the decomposition of the isotropic state [Eq. (S1)], it can be shown that only with probability

$$p'_{bc} = p_{ab}p_{ac}, \tag{S6}$$

or

$$\frac{4F'_{bc} - 1}{3} = \frac{4F_{ab} - 1}{3}\frac{4F_{ac} - 1}{3}, \tag{S7}$$

can a maximally entangled state be established directly between Bob and Charles. Otherwise, a completely mixed state is obtained. Considering the exponential dependence of p on the distance [Eq. (S2)], this equates to having an "effective" distance, $d_{ab} + d_{ac}$, between Bob and Charles.

Note that flying qubits are assumed to be abundant (as long as they can be constantly heralded [10]). Therefore, we ignore the rate efficiency and focus on the quality (fidelity) of the flying qubits. Assume that there already exists a channel connecting b and c, with distance d_{bc}. Given two channels of (effective) distances d_{bc} and $d_{ab} + d_{ac}$, the shorter one consistently yields higher-fidelity flying qubits. Consequently, only the shorter link needs to be retained. This leads to the *reduction rule*:

$$d'_{bc} = \min\{d_{bc}, d_{ab} + d_{ac}\}. \tag{S8}$$

At first glance, Eq. (S8) might not appear to enhance fidelity. Suppose the nodes a, b, and c are placed in a Euclidean space with all three quantum channels of Euclidean distances, d_{ab}, d_{bc}, and d_{ac}, established. The triangle inequality dictates $d_{bc} < d_{ab} + d_{ac}$, indicating that $d_{ab} + d_{ac}$ is always longer than the direct channel between b and c. However, the enhancement is hidden in two scenarios. Firstly, if, for some reason, a channel between b and c cannot be established, then $d_{bc} \to \infty$. In this case, Alice, acting as the relay, will significantly reduce the effective distance between Bob and Charles to a finite value $d_{ab} + d_{ac}$. Another possibility arises when Alice is not a single node but represents a connected component, where the links are perfectly entangled (in the limit $\epsilon \to 0$). Consequently, the real distances of these perfect links become inconsequential, as the flying qubits can be perfectly teleported from one end to another. Thus, the effective distance $d_{ab} + d_{ac}$, disregarding the path routing length within component a, could actually be smaller than the real distance d_{bc}.

It is worth noting that the quantum relay operation operates independently of quantum memories and does not impact the overall time complexity. However, one might wonder about the potential utility of quantum memories within the isolated component. Here, we demonstrate that, to the first-order approximation ($\epsilon \to 0$), leveraging quantum memories within the isolated component does not enhance the quantum relay feature.

Consider the scenario where Alice possesses m memories that can be utilized. This allows us to consider the following procedure: we initiate distillation between Alice and Bob, as well as between Alice and Charles, and then

swap the two distilled pairs to establish a direct pair between Bob and Charles, the fidelity F'_{bc} of this final pair (in the limit as $F \to 1$) is given by [Eq. (S7)]:

$$1 - F'_{bc} \simeq (1 - F_{ab}) + (1 - F_{ac}) , \tag{S9}$$

Here, F_{ab} (F_{ac}) represents the fidelity of the two distilled pairs between a and b (a and c):

$$1 - F_{ab} \simeq \frac{3}{4} m^{-\alpha} \frac{d_{ab}}{d_0} ,$$
$$1 - F_{ac} \simeq \frac{3}{4} m^{-\alpha} \frac{d_{ac}}{d_0} . \tag{S10}$$

However, this new fidelity F'_{bc} is identical to directly swapping m pairs between Bob and Charles (through Alice) and then distilling them, resulting in a fidelity F' given by

$$1 - F' \simeq \frac{3}{4} m^{-\alpha} \frac{d_{ab} + d_{ac}}{d_0} . \tag{S11}$$

A straightforward comparison yields $F'_{bc} = F'$. In other words, in the $\epsilon \to 0$ limit, distilling m pairs between a and b (a and c) and then swapping is *equivalent* to swapping m pairs from b to c (through a) and directly distilling them between b and c. However, the latter approach offers the advantage of not requiring quantum memories within Alice.

III. TIME COMPLEXITY OF α-PERCOLATION IN ONE DIMENSION

As a proof-of-concept, here we consider α-percolation in one dimension, illustrating how strategic utilization of distributed memories can enhance the connectivity of a one-dimensional network—within *subexponential time complexity*:

Denote $f(n)$ as the worst-case time complexity for establishing a perfectly entangled pair ($\epsilon \to 0$) within a component of size $\sim n$. The worst-case scenario corresponds to establishing a link near the *mid point* of the component. Therefore, consider two components, each sized $\sim n/2$, and establishing a link through their nearest nodes. α-percolation requires utilizing memories not only within the two nearest nodes but also distributed across the respective components, mandating the employment of our introduced remote distillation scheme. We also assume $m = 1$ w.l.o.g., or any constant that does not scale with n.

Initially, the flying qubits are teleported from the nearest nodes to other nodes within the two components and stored in the distributed memory qubits. The total high-entanglement links spent for this task amounts to

$$2\left[(n/2-1)+(n/2-2)+\cdots+1\right] \sim n^2, \tag{S12}$$

where $(n/2-1)$ is the number of links needed to teleport one flying qubit from the nearest node to the farthest node within one $n/2$-sized component; $(n/2-2)$ is to the second farthest node; and so on. Consequently, the time complexity of rebuilding these links is approximately $O(n^2)f(n/2)$, where $f(n/2)$ denotes the worst-case time complexity of rebuilding a link within a component of size $n/2$.

Subsequently, remote gate operations (CNOT gates, specifically) are required to act on these memory qubits. The total number of links utilized for this purpose is:

$$2\left[1\,(n/4)+2\,(n/8)+4\,(n/16)+\cdots+n/4\,(1)\right] \sim n\log_2 n. \tag{S13}$$

Here, $1(n/4)$ denotes the total count of high-entanglement links required during the first distillation round within one component, involving the teleportation of $n/4$ CNOT gates between every other pairs of nodes separated by a single link; for the second round, $2(n/8)$ specifies the requirement, with $n/8$ CNOT gates needing teleportation between nodes that are two links apart; and so on. Consequently, the time complexity of rebuilding these links approximates to $O(n\log_2 n)f(n/2)$.

Finally, a careful manipulation of the remote distillation process directly produces the distilled high-fidelity pair between the two nearest nodes. Combining these operations yields a total time complexity $f(n)$ given by:

$$f(n) \sim O(n^{-\log_2 p}) + \left(n^2+n\log_2 n\right)f(n/2), \tag{S14}$$

where the first term represents the time complexity of parallel distillation using memories, while the second term accounts for the compensation of expended links for all remote teleportation purposes. Taking the logarithm of the equation and assuming $f(n) \gg n^{-\log_2 p}$, we derive:

$$\frac{\ln f(\ln n) - \ln f(\ln n - \ln 2)}{\ln 2} \simeq \frac{2}{\ln 2}\ln n, \tag{S15}$$

which yields $\ln f \simeq (\ln 2)^{-1}(\ln n)^2$, or $f(n) = O(n^{\log_2 n})$, indicating subexponential time complexity.

Transitioning to higher dimensions, we anticipate even lower time complexity. This is since the depth of a component of size n will be less than n in higher dimensions. Consequently, the coefficient of the second term in Eq. (S14) could be smaller than n^2. However, achieving this necessitates careful path routing of teleportation within the component.

In higher dimensions, $f(n)$ denotes the time complexity of establishing a connected component of size $\sim n$, which is usually sparse. To construct a dense component, at most $\sim n^2$ links are needed. Thus, the worst-case time complexity is pushed to $n^2 f(n)$, which remains subexponential in n. Typically, the time complexity can take different subexponential forms based on the required connectivity density of the component.

Finally, there is also a practical caveat: for effective utilization of high-entanglement links within a connected component at any given time, it is advantageous to store these links into memory qubits as well. Nonetheless, this only demands an additional constant number of memories. Therefore, these additional memories have no bearing on the asymptotic results discussed above.

IV.   REDUCTION ON ISOLATED COMPONENTS IS OPTIMAL

We claim that applying the reduction rule only on *isolated* connected components can achieve the optimal connectivity. An isolated component is defined as when the range of the component fails to reach any of the component's neighbors. Additionally, it is only necessary to apply the reduction rule a single time to a component, immediately after it becomes isolated.

To show this, consider an isolated component b that has range r_b. It is clear that r_b cannot grow larger. This is because by the definition of isolated components, for any neighbor c of the component b, we must have $d_{bc} > r_b$. Therefore, the α-percolation criterion $d_{bc} < \min\{r_b, r_c\}$ will remain unsatisfied for r_b, inhibiting further growth of the size of b. The only exception is if a later reduction rule shortens the distance from b to c, denoted as d'_{bc}, after acting on a common neighbor a of both b and c. Suppose that now b can reach c. As a result, $r_b > d'_{bc}$. However, according to the reduction rule [Eq. (S8)], this subsequently implies either $r_b > d_{bc}$ or $r_b > d_{ab} + d_{ac} > d_{ab}$, implying b could reach either a or c *before* reduction on a. This contradicts the initial assumption of b being isolated.

Hence, we conclude that *once a connected component becomes isolated, it remains isolated and cannot forge links with any other components.* Consequently, the reduction rule needs to be applied only once to any isolated component. This is because once a component is isolated, it will not merge with others or gain new neighbors, thus no new shortcuts will be generated.

After component a is identified as isolated, it should be "removed" from the percolation process of the rest of the network after applying reduction to it. This removal means that when other nodes are tested whether they are isolated, they no longer count a as a neighbor. As a result, other nodes may become isolated now after the removal of a. Ultimately, this process continues until all nodes are isolated, reaching the final state. Of course, this removal is only conceptual. It does not imply that nodes within isolated components are physically erased. The nodes are still linked with other nodes in the same isolated component.

Now we demonstrate that *applying reduction to isolated components is more beneficial than applying it to non-isolated ones.* Note that a component always produces more efficient shortcuts when getting merged, so in general it is beneficial to wait until the component cannot merge any more, becoming isolated. The critical question, however, is whether reducing a component a before it is isolated can offer a *timely* advantage, potentially facilitating the merging of other components before those components become isolated. This scenario is impossible. If two components, b and c, could benefit from a shortcut d'_{bc} created by a, then it must be that $r_b > d'_{bc}$ and $r_c > d'_{bc}$. This implies that either both $r_b > d_{bc}$ and $r_c > d_{bc}$ are true, indicating b and c do not require a's shortcut, or both $r_b > d_{ab} + d_{ac} > d_{ab}$ and $r_c > d_{ab} + d_{ac} > d_{ac}$ are true, suggesting b and c cannot be considered isolated before a is removed. Therefore, if b and c need a shortcut from a, they can afford to wait until a is isolated. Of course, once a becomes isolated, the reduction rule should be applied immediately on a, before a is removed. Given that all nodes will eventually become isolated, this principle applies universally.

V.   SEQUENCE OF CONDUCTING THE GRAPH-MERGING RULES

Now we investigate whether the sequence of implementing the two graph-merging rules holds significance, arguing that, in fact, the order does *not* affect the outcome:

(1) The *contraction rule*, as expressed by Eq. (S5), is commutative. Consequently, the enhanced range $r(s)$ of a node within a component solely depends on the component size s, irrespective of the specific order of contracting different nodes within the component. The whole process is therefore equivalent to a component-finding algorithm, which can be simply done using, e.g., a depth-first search. Also, note that the distance between two components a and b is defined as the distance between their nearest nodes, i.e., $d_{ab} = \min_{i \in a, j \in b} d_{ij}$. This again does not depend on the specific order of applying the contraction rule to the two components either. Consequently, these two properties together establish the effective-node picture, where a connected component can be equivalently regarded as an effective node with range $r(s)$.

(2) Similarly, the minimum operation in the *reduction rule* [Eq. (S8)] is also commutative. Thus, the sequence in which isolated effective nodes are reduced also does not influence the outcome. In fact, given an isolated effective node a, we do not even actually need to remove a and add a "shortcut" d'_{bc} between every pair of its neighbors b and c. Instead, we can simply run a shortest-path algorithm, such as Dijkstra's algorithm, to identify the shortest path length between b and c, whether through the relay a or not. When there are multiple isolated effective nodes, this shortest-path approach can significantly reduce the computational complexity by avoiding the potential overload of shortcuts established throughout the network.

(3) The only remaining point that requires investigation is when both the contraction and reduction rules are involved. Given the requirement that reduction only happens for isolated components, we have posited that this approach yields optimal connectivity. Then, the question becomes whether altering the sequence of these rules might prevent certain nodes, say i and j, which would otherwise merge optimally, from being able to do so. This scenario, however, is impossible. If i and j are merged in the final state, they cannot become isolated mid-process, as a continuous path for their eventual convergence always exists, which means i will always have a neighbor k such that $r_i > d_{ik}$, hence i cannot be isolated. The only exception is that d_{ik} was originally larger than r_i but was later shortened by a reduction rule on i and k's common neighbor, say l. Yet, according to Eq. (S8), this situation still ensures that $r_i > d_{il} + d_{lj} > d_{il}$. Thus, under no circumstances can i become isolated. The same argument also works for j. And finally, contraction on i (or j) with other nodes also does not impact i and j's connectivity: due to the "minimum rule" definition of the distance between two components, $d_{ab} = \min_{i \in a, j \in b} d_{ij}$, node i's shortest distance to j will only decrease after merging with other nodes. Eventually, i and j must be merged in the final state.

Drawing from these observations, we argue that the sequence in which the contraction and reduction rules are applied is inconsequential. The final state of configuration—how nodes are distributed across components—remains unchanged. Our algorithm initially applies contraction rules to the maximum number of nodes feasible, then proceeds to reduce all isolated components to add shortcuts. This cycle is repeated until the final configuration is established.

Note that for many traditional SDRG rules, the sequence of applying the rules plays a crucial role [37]. In SDRG, different merging orders of sites and bonds could often yield distinct outcomes. Moreover, SDRG rules are typically more approximate away from the critical point. This is in contrast to our α-percolation rules, which are more generic, applicable regardless of whether at criticality or not, and not influenced by the order in which they are performed.

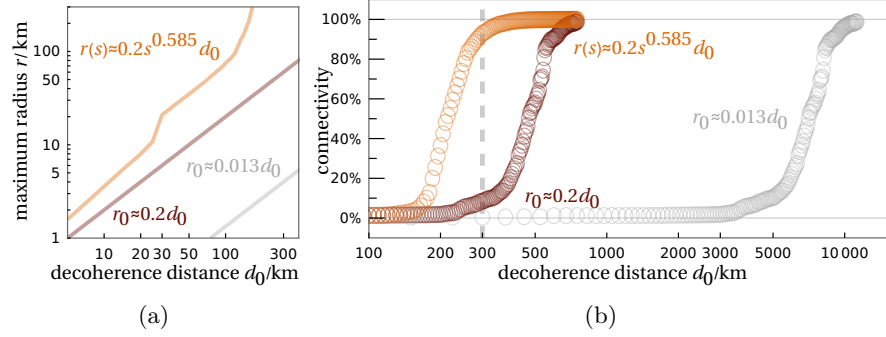# VI. DETAILED ANALYSIS ON REAL QUANTUM NETWORKS

(a) (b)

FIG. S3: Different memory utilization strategies implemented on Sparkle's pan-European fiber network. (a) From right to left: absence of memory (gray), local memory utilization at the node level (brown), and distributed memory utilization at the component level (orange). Enabling distributed memories enhances the maximum range achievable by a node. (b) Correspondingly, in the absence of quantum memories, the decoherence distance d_0 must surpass ~ 8000 km to ensure sufficient connectivity (above 90%) among nodes. Incorporating quantum memories already yields substantial local improvements at the individual node level, reducing the required d_0 to just ~ 600 km. Our model further enhances this by leveraging distributed quantum memories, cutting down the necessary d_0 to ~ 300 km— a distance now within the ambit of current laboratory capabilities. The fidelity bound for each link is set at $1-\epsilon = 99\%$. Each node is assigned $m \approx 102$ quantum memories such that $m^{\alpha^*} \approx m^{0.585} = 15$. The comparison between local (brown) versus distributed (orange) memory usage is also illustrated in Fig. 3(b) of the main text.

   The original Sparkle's pan-European fiber network [28] has an average length scale of approximately ~ 500 kilometers, surpassing the current laboratory limit of $\beta = d_0 \ln 3 \approx 330$ kilometers. Due to *entanglement sudden death* [27], it is impossible—via any combination of quantum communication protocols—to establish entanglement across such a typical length scale within the original fiber network. This situation is reminiscent of the role of finite-temperature for quantum phase transitions, where the inverse temperature β introduces a finite length scale, capping the correlation length [31].

   Hence, the introduction of quantum repeaters [29] becomes necessary to reduce the length scale. To simulate this process, we altered the topology of the original fiber network by segmenting cables into shorter, randomly distributed segments following a Poisson distribution in length, with an average around 50 kilometers. These newly introduced nodes, which concatenate these segments, effectively function as full-fledged quantum repeaters. Consequently, the resultant network comprises 692 nodes (including the repeaters) and 733 links. We set $d_{ij} \to \infty$ for any pair of nodes i and j not directly connected by a cable.

   In our simulations, we assumed that each node was equipped with approximately $m \approx 102$ quantum memories, yielding $m^{\alpha^*} \approx m^{0.585} = 15$. The fidelity bound was set at $1-\epsilon = 99\%$. We examined three scenarios: (1) no memory utilization, where each node's range $r_0 \simeq 4\epsilon d_0/3 \approx 0.013d_0$ remains fixed; (2) local memory utilization only at the node level, resulting in an increased range for each node to $r_0 \simeq 4m^{\alpha^*}\epsilon d_0/3 \approx 0.2d_0$, albeit still remaining fixed; (3) distributed memory utilization at the component level, facilitated by the synergy between quantum communication protocols, leading to a size-dependent range $r(s) \simeq 4\epsilon m^{\alpha^*} s^{\alpha^*} d_0/3 \approx 0.2s^{0.585}d_0$. As d_0 increases, Fig. S3(a) illustrates distinct behaviors for the three scenarios. Notably, as nodes are merged into larger components, the maximum $r(s)$ (i.e., of the largest component) experiences a nonlinear increase. Consequently, this enhancement in range contributes to better network connectivity, as shown in Fig. S3(b).